MODULAR MULTILEVEL CONVERTER WITH STATE-FEEDBACK CONTROLLER FOR HARMONICS SUPPRESSION

A.U. Lawan[1], A.Abdulkarim[2], G.S. Shehu[2], A. Kunya[2], I.S Madugu[3]
[1] Department of Electrical Engineering, University of Nottingham, Malaysia.
[2] Department of Electrical Engineering, Ahmadu Bello University Zaria, Nigeria.
[3] Department of Electrical Engineering, Kano University of Sci. & Tech, Nigeria.
[1] kecx4aua@nottingham.edu.my

Keywords: –
Controller.
Current reference,
Modular,
Multilevel ,
state-feedback,

Article History: –
Received: January, 2019.
Reviewed: April, 2019
Accepted: August, 2019
Published: September,2019

ABSTRACT

Control of submodule capacitor voltages and the circulating current within modular multilevel converter (MMC) is essential to MMC performance. The circulating current has an influence on the losses, rating of the power devices and voltage ripple. The circulating current tends to have csurrent harmonics due to the voltage disturbance on the submodule capacitor voltages. To decrease the influence of the harmonics for an improved control of the submodule capacitor voltages, a voltage control approach by suppressing the current produced by the voltage disturbance is introduced. The approach is implemented using a virtual-impedance compensation that increases the voltage reference of the averaging voltage control of the circulating current reference in order to decrease the impact of the disturbance. The improved capacitor voltage control produces a new circulating current reference to a state-feedback controller provided to control the measured circulating current using a linear quadratic regulator to shape the gain of the controller. The main advantage of the approach is that it allows wideband ripple suppression without having knowledge of the harmonics frequencies; this is unlike the usual multiresonant controllers which are restricted to the particular knowledge of frequencies. From the results obtained, the control using the proposed method has the advantages of an improved voltage control, reduced capacitor voltage ripple and harmonics compared to the conventional proportional integral controllers. The results from the proposed method and the conventional method are shown in a simulation. Finally, the experiment results are presented to verify the simulation.

1. INTRODUCTION

Modular multilevel converter (MMC) technology is widely viewed as the recent configurations in power electronics industries. Their applications are possible due to multilevel controlled and balanced voltages that are shared among the switches [1–3]. There are many control schemes such as direct control, power synchronization, and direct-quadrature control, among others, applied to MMCs [5]–[7]. MMC applications for stability and control have been employed based on different modulation techniques for a different level of stacked cells [8–10]. alancing control of the stacked cells have been achieved using different methods [11–15], [16]. However, for an MMC increasing the stacked cells increases the switching frequency and voltage ripples. Depending on a number of the levels, this would in turn increase the control complications such as the capacitors voltage balancing and voltage disturbances that produce harmonic ripples. However, the multilevel feature gives the advantage of having a transformer-less system for an improved efficiency [17–19]. The voltage balancing control of the capacitors has an effect on the quality of the MMC outputs. The voltage disturbance that can arise due to poor voltage balancing control produces harmonics [20]. The voltage variation from within the MMC makes the circulating current to have ripple components [15]. The use of the PI-controllers in the internal control of the MMC is one of the common solutions to obtain a zero-static error in controlling the circulating current. However, PI-controllers have a little effect in suppressing the harmonic voltage unless high-gain high-order controllers, such as resonant controllers are used with the PI-controllers within the control bandwidth [21]. Control of capacitor voltages have

been achieved using different approaches [22],[23], [24]. Cisneros et al. [25] studied the global tracking of a bilinear system which was assumed linear time-invariant (LTI). The system was applied to a Boost-MMC and the control was to track the desired currents. The control was to produce a control method in the rotating (abc) frame [27]. This is unlike the classical (dq0) frame method [28]. The control resulted in good tracking performance between the desired and the measured currents instead of the usual control regulation. However, the tracking was complex due to the bi-linearity feature [25]. To decrease the impact of voltage variation among the capacitors, the use of a virtual-impedance can be used as an option either with a time integral or a time derivative to suppress any unwanted current, thus reducing the harmonics without increasing the size of the capacitors. The use of the derivative with a virtual-impedance can increase system impedance. However, with the presence of noise, , the derivative term amplifies the noise [29].

To minimize the amplified noise generated by the derivative term, a low pass filter (LPF) can be used. However, LPF add delay and cost[21]. This paper considers the presence of the voltage disturbance and employs the closed-loop virtual-impedance concept. The closed-loop will be applied to increase the MMC internal impedance and lessen the amount of the unwanted current produced by the voltage disturbance, therefore, improving the capacitor voltage control. The improved control will provide a new circulating current reference. The advantage of this method is that it does not need any additional sensing devices to achieve its implementation as it uses the available measurement values in the system. Moreover, its application is not restricted to particular frequencies in order to achieve harmonics suppression. Furthermore, the model of the MMC presented is found to be inadequate in handling the impact of voltage disturbance. This will be illustrated in Section II of this paper. Therefore, another contribution of the proposed method is that it modifies the MMC model to handle the impact of the voltage disturbance, thus enhances the practical applications of the model. This can be achieved with simplicity and without the use of any additional filter such as in [30],[31].

2. MECHANISM OF CIRCULATING HARMONIC CURRENT AND STATE-FEEDBACK CONTROL

Fig. 1 gives the three-phase MMC system, where *If* and *Vc* are the MMC output three-phase current and voltage respectively. *Vf* is the reference voltage, *Lf* is the coupling filter inductance, *Rf* is the coupling filter series resistance, *Vdc* is the direct current (DC) link voltage, *Lr* is the arm inductance and *Rr* is the arm resistance. Applying Kirchhoff's principle on any leg/phase with respect to node *n*, the mathematical relations between any phase output current *Ik* , the lower and upper arm currents (*Ikp* and *Ikn*), and the circulating current *Icirk* are:

$$I_{kp} = I_{cirk} + \frac{I_k}{2};\ I_{kn} = I_{cirk} - \frac{I_k}{2} \qquad (1)$$

$$V_{ckn} + V_{ckp} = V_{dc} - 2V_{cirk};\ V_{cirk} = L_r \frac{dI_{cirk}}{dt} + R_r I_{cirk} \qquad (2)$$

The sub-script *k* represents any of the three-phases (u, v or w). *Vcirk* is the differential-mode voltage, *VCkp* and*Vckn* are the upper arm and lower arm output voltages respectively.

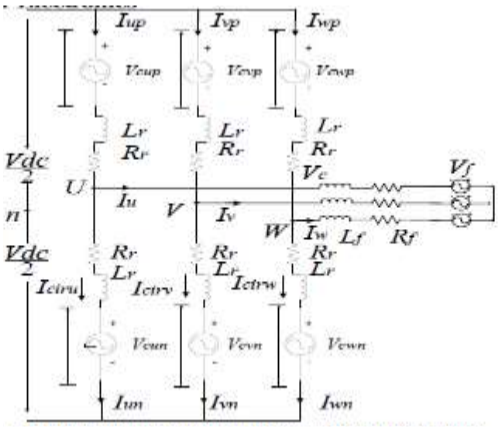

Fig. 1. MMC in a three-phase configuration.

Based on (1) and (2), the regulation of the circulating current and the output voltage *Vck* in (5) can be achieved by controlling *Ikp* and *Ikn* , and the *VCkp* and *VCkn* in (3) and in (4) respectively

$$V_{Ckp} = \frac{1}{2}V_{dc} - V_{Ck} \quad (3)$$

$$V_{Ckn} = \frac{1}{2}V_{dc} + V_{Ck} \quad (4)$$

$$V_{Ck} = \frac{1}{2}V_{dc*}\, M \sin(\omega t) \quad (5)$$

M is the modulation index and ω is the frequency. I_k in term of its peak value I_o and the phase angle φ_k is as $I_k = I_o \cdot \sin(\omega t - \varphi_k)$ (6)

Equations (3) and (4) present the arm voltages under ideal conditions. However, when the load current and the circulating current due to the presence of the inductor *Lr* in the MMC leg flow through the submodule capacitors, the capacitor voltages fluctuate. Hence a control approach has to be employed to keep the voltages near to their references [32],[33].

The circulating current is in form of a DC component I_{dc} and the harmonic components *in* of nth order and is as

$$I_{cir} = \frac{1}{3}I_{dc} + \sum_{n=1}^{\infty} i_n \quad (7)$$

Based on (5)-(7), the instantaneous power and active energy stored in the arms comprising a number of SM capacitor *C* are given in (8) and (9) respectively, and their relationship is given in (10) [21]:

$$\left.\begin{aligned} p_{arm-kp} &= \frac{1}{2}V_{dc}\left(1 - M\sin(\omega t)\right)\cdot\left(\frac{i_k}{2} + \frac{1}{3}i_{dc} + \sum_{n=1}^{\infty} i_n\right) \\ p_{arm-kn} &= \frac{1}{2}V_{dc}\left(1 + M\sin(\omega t)\right)\cdot\left(\frac{-i_k}{2} + \frac{1}{3}i_{dc} + \sum_{n=1}^{\infty} i_n\right) \end{aligned}\right\} \quad (8)$$

$$\left.\begin{aligned} W_{kp} &= \frac{1}{2N}CV_{Ckp}^2 \\ W_{kn} &= \frac{1}{2N}CV_{Ckn}^2 \end{aligned}\right\} \quad (9)$$

$$\left.\begin{aligned} \frac{dW_{kp}}{dt} &= \frac{C}{N}\cdot V_{dc}\cdot\frac{d}{dt}V_{Ckp} = p_{arm-kp} \\ \frac{dW_{kn}}{dt} &= \frac{C}{N}\cdot V_{dc}\cdot\frac{d}{dt}V_{Ckn} = p_{arm-kn} \end{aligned}\right\} \quad (10)$$

From (9-10) the voltage disturbances in the arms are:

$$\left.\begin{aligned} \Delta V_{Ckp} &= \frac{N}{2C}\int\left(1 - M\sin(\omega t)\right)\cdot\left(\frac{I_k}{2} + \frac{1}{3}I_{dc} + \sum_{n=1}^{\infty} i_n\right)dt \\ \Delta V_{Ckn} &= \frac{N}{2C}\int\left(1 + M\sin(\omega t)\right)\cdot\left(-\frac{I_k}{2} + \frac{1}{3}I_{dc} + \sum_{n=1}^{\infty} i_n\right)dt \end{aligned}\right\} \quad (11)$$

From (11), the arms voltages can be modified as

$$\left.\begin{aligned} V_{kp} &= \frac{1}{2}\left(1 - M\sin(\omega t)\right)\cdot\left(V_{dc} + \Delta V_{Ckp}\right) \\ V_{kn} &= \frac{1}{2}\left(1 + M\sin(\omega t)\right)\cdot\left(V_{dc} + \Delta V_{Ckn}\right) \end{aligned}\right\} \quad (12)$$

from (13), the total output voltage of the arms are:

$$V_{Ckp} + V_{Ckn} = V_{dc}\frac{1}{2}\left(\Delta V_{Ckp} + \Delta V_{Ckn}\right) + \frac{1}{2}M\sin(\omega t)\cdot \left(\Delta V_{Ckn} - \Delta V_{Ckp}\right) \quad (13)$$

Equation (13) can be written as in (14), where V_{kd} is the voltage variation that is responsible for the variation between the phase-k leg and the total SMs voltage values when the system is under normal control. Equation (14) shows that the variation can be practically assessed using the measured capacitor voltages and the dc link voltage value.

$$V_{kp} + V_{kn} = V_{dc} + V_{kd} \quad (14)$$

Based on the nearest level modulation (NLM) method, the following assumptions hold [34]:

1) Using capacitor selection, the individual capacitor voltages within the arms are controlled;

2) The switching frequency and the number of the SMs are large enough when compared to the waveform of the SM capacitor to make discretization effect negligible. The assumptions 1-3 creates an instantaneous amount of the inserted arm voltages $v_{kp,n} = N_{p,n}v_{ckp,n}^{\Sigma}$ through bypass/insert process of the SMs given in (15).

$$\left.\begin{aligned} V_{kp} &= N_p V_{ckp}^{\Sigma} = V_{dc}\underbrace{\frac{1}{2}\left(1 - M\sin(\omega t)\right)}_{V_{ckp}^{\Sigma}\ N_p} \\ V_{kn} &= N_n V_{ckn}^{\Sigma} = V_{dc}\underbrace{\frac{1}{2}\left(1 + M\sin(\omega t)\right)}_{V_{ckn}^{\Sigma}\ N_n} \end{aligned}\right\} \quad (15)$$

Equation (15) can be written as

$$\left.\begin{aligned} V_{kp} &= N_p V_{ckp}^{\Sigma} = \frac{V_{dc}}{2} - V_{ck} - V_{cirk} \\ V_{kp} &= N_p V_{ckp}^{\Sigma} = \frac{V_{dc}}{2} - V_{ck} - V_{cirk} \end{aligned}\right\} \quad (16)$$

where *Np* and *Nl* are the indices of insertion in the upper and lower respectively. Putting (16) into (2) yields:

$$\frac{dI_{cirk}}{dt} = -\frac{R_r}{2} I_{cirk} - \left(\frac{N_p}{2L_r} V_{ckp}^{\Sigma} - \frac{N_n}{2L_r} V_{ckn}^{\Sigma} \right) + \frac{V_{dc}}{2L_r} \quad (17)$$

The rate of change of the arm voltages are as

$$\frac{dV_{ckp}^{\Sigma}}{dt} = \frac{N.N_p.I_{kp}}{C} \; ; \; \frac{dV_{ckn}^{\Sigma}}{dt} = \frac{N.N_n.I_{kn}}{C} \quad (18)$$

From (17) and (18), the MMC internal dynamics can be as

$$\underbrace{\frac{d}{dt}\begin{bmatrix} I_{cirk} \\ V_{ckp}^{\Sigma} \\ V_{ckn}^{\Sigma} \end{bmatrix}}_{\dot{x}} = \underbrace{\begin{bmatrix} -\frac{R_r}{L_r} & -\frac{N_p}{2L_r} & -\frac{N_n}{2L_r} \\ \frac{N.N_p}{C} & 0 & 0 \\ \frac{N.N_n}{C} & 0 & 0 \end{bmatrix}}_{A} \underbrace{\begin{bmatrix} I_{cirk} \\ V_{ckp}^{\Sigma} \\ V_{ckn}^{\Sigma} \end{bmatrix}}_{x} + \underbrace{\begin{bmatrix} \frac{V_{dc}}{2L_r} \\ \frac{N.N_p}{2C} I_k \\ -\frac{N.N_n}{2C} I_k \end{bmatrix}}_{u} \quad (19)$$

The system in (19) is a third-order system where *x* is the state vector and *u* is the input vector. *A* is the state matrix. Due to the presence of periodically varying

quantities: *Np* and *Nn* , the system is time varying [34]. Equation (19) can be applied to a high switching carrier shifted pulse width modulation (CSPWM) method with the following voltage control [21, 35] conditions:

1) Using the individual balancing control the individual voltages of the capacitors within the arms are controlled to their reference and V_{dc} is at a fixed value;

2) The voltages in the arms are controlled in such a way there is no voltage discrepancy between them;

3) The averaging voltage control is implemented such that the averaging-capacitor voltage V*Ck* of each phase leg tracks the reference voltage V* *Ck* . This will impose the circulating current to track its reference.

3. PROPOSED VIRTUAL-IMPEDANCE LOOP FOR A STATE FEEDBACK CONTROL OF CIRCULATING CURRENT WITH HARMONICS SUPPRESSION

The voltage disturbance explained in Section II can cause the MMC to produce ac-harmonics which are undesirable. Controllers such as the repetitive controllers [21] can be employed. Another approach to mitigate the impact of the voltage disturbance is to employ the concept of state observer such as in [36]. A state observer can estimate the state of the system considering the disturbance and form a model that has the capability to cancel the disturbance effect. However, the estimation might come with error, thus full cancellation may not be feasible [36].

In this paper, the concept of a state-feedback controller will be employed to regulate the circulating current. And as well, a virtual-impedance *Zv* will be employed by integrating over a virtual capacitance *Cvir* (*Zv*(*s*) □1/ *sCvir* where s is the Laplace operator) to produce an opposing virtual voltage *Vcom* that will decrease the influence of the voltage disturbance for an improved harmonics suppression without the use of a time-derivative. The relationship between V_{kd} of (14), V_{kd_2f} as dominant second-order harmonic voltage component of V_{kd} with its corresponding current I_{kd_2f} and the peak value I_{kd} can be written as follows [37]:

$$\begin{aligned} V_{kd} &= V_{dc}\frac{1}{2}\left(\Delta V_{Ckp} + \Delta V_{Ckn}\right) + \frac{1}{2} M \sin(\omega t)\cdot\left(\Delta V_{Ckn} - \Delta V_{Ckp}\right) \\ &= V_{kd\_2f}; \quad I_{kd\_2f} = I_{kd}\cos(2\omega t) \end{aligned} \quad (20)$$

where V_{kd_2f} excites the circulating current at twice fundamental frequency to produce the second order circulating current I_{kd_2f} which is the main current passing through the MMC leg besides the dc current. The circulating harmonic current will then produce 4th, 6th… 2kth harmonic current by itself.

Note that it is based on simplicity and to show the impact of the voltage disturbance in (21) and (22) V_{kd} is reduced to $V_{kd}-2f$ [37], [21]. In addition, other high-frequency harmonic voltage in form of a switching voltage ripple that is usually super-imposed on the dc-link voltage can also be added as part of the disturbance in (20) for some applications.

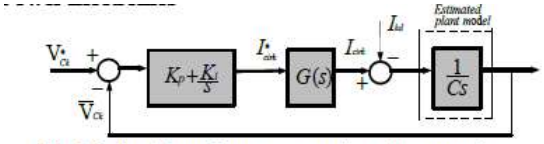

Fig. 2. Reduced form of an average capacitor voltage control

Considering the voltage disturbance $V_{kd}-2f$ of (20), (15) canbe expanded and written as in (21) and (24).

$$V_{Ckp} = N_p V_{ckp}^{\Sigma} = \underbrace{V_{dc}}_{V_{Ckp}^{\Sigma}} \underbrace{\frac{1}{2}(1-M\sin(\omega t))}_{N_p} + \underbrace{\frac{V_{2f}}{2}\sin(2\omega t)}_{V_{kd\_2f}} \quad (21)$$

$$V_{Ckn} = N_n V_{ckn}^{\Sigma} = \underbrace{V_{dc}}_{V_{Ckn}^{\Sigma}} \underbrace{\frac{1}{2}(1+M\sin(\omega t))}_{N_n} + \underbrace{\frac{V_{2f}}{2}\sin(2\omega t)}_{V_{kd\_2f}} \quad (22)$$

Equation (21) and (22) show that the model obtained in (19) is insufficient to handle voltage disturbance. This means the model applications can be enhanced when the impact of the peak value I_{kd} in (20) is reduced. Therefore, the use of the virtual-impedance loop voltage as opposing signal will mitigate the impact of the peak current disturbance I_{kd}.

To verify the impact of the virtual-impedance with simplicity, a reduced model of SM capacitor voltage control with a voltage PI-controller in Fig. 2 will have *Kp* as the proportional gain, *Ki* as the integral gain. *G*(*s*) is the internal circulating current control transfer function for a plant *Gp*(*s*) assuming its proportional gain *Kc* only. Note that Fig. 2 is only considered to mathematically check the impact of the virtual-impedance. Fig. 3 shows the full control representation of Fig. 2 based on the lower arm with insertion index *Nn* [38]. The transfer functions and the control variables in Fig. 2 are as

$$G(s)=\frac{K_c G_p}{1+K_c G_p};\ G(s)=\frac{1}{L_r s+R_r};$$

$$\overline{V}_{Ck}(s)=\frac{K_c(K_p s+K_i)}{L_r C s^2+R_r C s+K_c C s+K_c(K_p s+K_i)}\overline{V}^{*}_{Ck}(s) - \frac{L_r s+R_r+K_c}{L_r C s^2+R_r C s+K_c C s+K_c(K_p s+K_i)} I_{kd}(s) \quad (23)$$

From (23), the system can be modelled as:\

$$\overline{V}_{Ck}(s)=h(s).\overline{V}^{*}_{Ck}(s)-Z_o(s)I_{ok}(s) \quad (24)$$

J (*s*) is the transfer function of the reference voltage-toaverage voltage. *Zo*(*s*) is the impedance transfer function. From (24), it is obvious that the impedance *Zo*(*s*) will have an effect on the SM capacitor voltage control. To provide the desired impedance $Z_v(s)$ for an improved control with reduced harmonics, the reference voltage $\overline{V}^{*}_{Ck}(s)$ can be obtained from new reference voltage $\overline{V}^{i*}_{Ck}(s)$ that is related to $I_{ok}(s)$ as

$$\overline{V}^{*}_{Ck}(s)=\overline{V}^{i*}_{Ck}(s)-Z_v(s)I_{ok}(s) \quad (25)$$

Ck s is the new averaging voltage reference.

Putting (25) into (24), the dynamic equation is as

$$\overline{V}_{Ck}(s)=h(s).\overline{V}^{'}_{Ck}(s)-(h(s)Z_v(s)+Z_o(s))I_{ok}(s) \quad (26)$$

where $Z_{ov}(s)=(h(s)\,Z_v(s)+Z_o(s))$ is the new transfer function of the total internal impendence.

From (26), it can be seen that an improved impedance $Z_{ov}(s)$ can be obtained by adding to the original impedance $Z_o(s)$, a virtual-impedance term $J(s)Zv(s)$.Integrating the current I_{kd} over a virtual capacitance C_{virc} produces a compensation voltage $V_{com}(s)$ as

$$V_{com}(s)=\frac{I_{kd}(s)}{sC_{virc}}=I_{kd}(s)G_{com}(s) \quad (27)$$

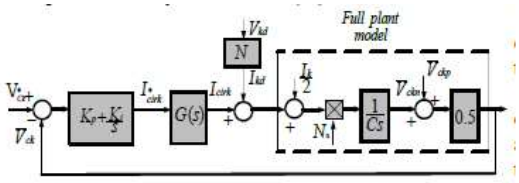

Fig. 3. Full model of average capacitor voltage control

Where $G_{com}(s)$ is the virtual compensator. Based on Fig. 3 and (27), the control relationship between the measured average voltage $\overline{V}_{Ck}(s)$ and the voltage disturbance $V_{kd}(s)$ can be as follows:

$$\frac{\overline{V}_{Ck}(s)}{V_{kd}(s)}; = \frac{G_{com}\dfrac{G(K_p s + K_i)}{s} - N}{1 + \left(\dfrac{G(K_p s + K_i)}{s}\right)/2C} \tag{28}$$

From (28), it is clear that the influence of the voltage disturbance on the measured capacitor voltages in the control loop of Fig. 3 can be suppressed by choosing the value of the virtual capacitor to satisfy the relation of (29).

$$\frac{1}{sC_{virc}} \approx \frac{N}{\left(\dfrac{G(K_p s + K_i)}{s}\right)} \tag{29}$$

Thus, an improved reference current can be as

$$i^*_{cirk} = K_1\left(V^*_{Ck} - V_{com.} - \overline{V}_{Ck}\right) + K_2\int\left(V^*_{Ck} - V_{com.} - \overline{V}_{Ck}\right)dt \tag{30}$$

The PI-controller in (28) will be replaced with a state-feedback controller to apply the proposed method using model of (19). The state-space model of the internal dynamics is:

$$\dot{x}_r = A_r x_r + B_r u \tag{31}$$

$$A_r = \begin{bmatrix} -\dfrac{R_r}{L_r} & -\dfrac{N_p}{2L_r} & -\dfrac{N_n}{2L_r} \\ \dfrac{N \cdot N_p}{C} & 0 & 0 \\ \dfrac{N \cdot N_n}{C} & 0 & 0 \end{bmatrix} \tag{32}$$

$$B_r = \begin{bmatrix} 1 \\ 1 \\ 1 \end{bmatrix};\ x_r = \left[i_{cirk}, v^{\Sigma}_{ckp}, v^{\Sigma}_{ckn} \right]^T. \tag{33}$$

$$\dot{x}_r = (A_r - B_r K)x_r \tag{34}$$

$$N_u = (1 - M\sin(\omega t)); N_l = (1 + M\sin(\omega t)) \tag{35}$$

Equation (32) is controlled in a discretized form using the gain $K_{\_aug.}$ shaped by a linear quadratic regulator (LQR) based on the control law:

$$u(k) = -K.\ x_r(k) \tag{36}$$

That minimizes the cost function

$$J_{LQR} = \sum_{k=0}^{\infty}(x_r^T(k) Q\, x_r(k) + u_r^T(k) \cdot R \cdot u(k) \tag{37}$$

where *R* and *Q* are the weighting matrices that can be determined based on Bryson's rule [30] and *K* is the gain of the LQR. Finally, the overall internal control with the associated controls is shown in Fig. 4. The capacitor voltage control: the average capacitor voltage control, arm balancing control and the individual control are employed as shown in Fig 4.

The voltage command *vcirk* can be either from the conventional average voltage control or from the proposed method as shown in Fig. 4. Both methods are independently compared. The gains *K*1 and *K* 2 in Fig. 4(a) and Fig. 4(b), and the gains of the inner current PI-controller in Fig. 4(a) can be obtained by pole-zero cancelation method [25] or by fuzzy algorithm [39, 40] among others. The voltage commands for the individual control and arm balancing control are *vkB* (*i*, *j*) and *vkA* shown in Fig 4(c) and Fig. 4 (d) respectively. The proportional controllers which are known to have rapid-error correction feature [41-44] with gains *K*3 and *K* 4can be employed for the individual and arm balancing controls respectively. Figure 4(e) shows the generation of the overall voltage command *ux* for the CSPWM of the MMC. The voltage symbols in Fig. 4 are obtained as follows:

$$\left.\begin{aligned} \bar{V}_{Ck} &= \frac{1}{2}\left(\bar{V}_{Ckp} + \bar{V}_{Ckn}\right); \bar{V}_{Ckp} = \frac{1}{N}\sum_{i=1}^{N} V_{Cki} \\ \bar{V}_{Ckn} &= \frac{1}{N}\sum_{j=N+1}^{2N} V_{Ckj}\ ; v_C^* = \frac{V_{dc}}{N} = V_{Ck}^* \end{aligned}\right\} \quad (38)$$

where $\bar{V}_{Ck}$ is the phase-k average capacitor voltage. $\bar{V}_{Ckn}$ and $\bar{V}_{Ckp}$ are the average capacitor voltage of the lower arm and upper arm respectively. V_{Cki} and V_{Ckj} are the voltages of the *i*th and *j*th SMs in the upper arm and lower arm respectively.

4. IMPLEMENTATION AND SIMULATION RESULTS

In this section, the proposed control implementation is presented, the control is done in a digital form using MATLAB/Simulink. The modulation is validated using a nine-level MMC proto-type with four submodules per arm. The modulation is done using carrier-shifted pulse width modulation at 2KHZ. This means the overall switching frequency is 16KHZ. The current discrete PI-controller in a data sampled form has been employed. The simulation has been carried out based on Table I of the obtained control parameters and Table II of the the system parameters. The system parameters include the arm resistance of *Rr*=0.4Ω, *Cvirc* =4mF and *Lr*=2mH.

The gains of the inner current controller are obtained based on the pole-zero cancellation using the MMC system parameters. The current controller resulted in an estimated bandwidth of 1200Hz and a phase margin of 160° from its frequency response. Similarly, the averaging capacitor voltage control for the conventional method has been employed based on the PI-control scheme. The PI-controller gains of the voltage control are also obtained based on the pole-zero cancellation technique. The frequency response analysis and the gain selections are carried out to establish a hitch-free interaction between the outer-loop voltage controllers, the inner-loop current controller and the virtual compensator. For the proposed method, the same PI-control in the outer-loop capacitor voltage control is employed. For the circulating current control, the LQR based state-feedback algorithm is employed. The control of the circulating current is carried out using the two methods: 1. the conventional method based on Fig. 4(a), and 2. the proposed method based on Fig. 4(b). A time–domain simulation of the two methods has been conducted.

Fig. 6 shows the circulating current control response based on the conventional PI–control and the virtual-impedance loop with the state-feedback control. It can be seen from Fig. 6(a) that during the control start-up, the current has an overshoot of not less than 1.2A at a time t=0.02 sec. and has reached its steady-state value of 0.5A at approximately 0.10 sec. The presence of harmonics in form of oscillations can be seen in both the measured circulating current and the reference circulating current. In the other hand, the state-feedback based control method has produced higher current overshoot of about 1.8 A which is slightly above that of the PI-based control current.

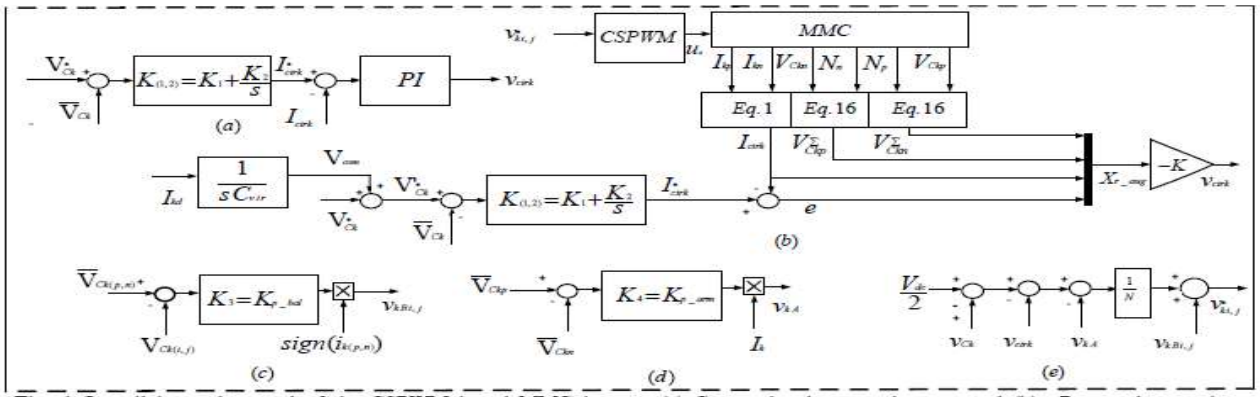

Fig. 4 Overall internal control of the CSPWM based MMC inverter (a) Conventional averaging control (b) Proposed averaging control connected to the MMC (c) Individual voltage balancing control (d) Arm balancing control (e) overall voltage command

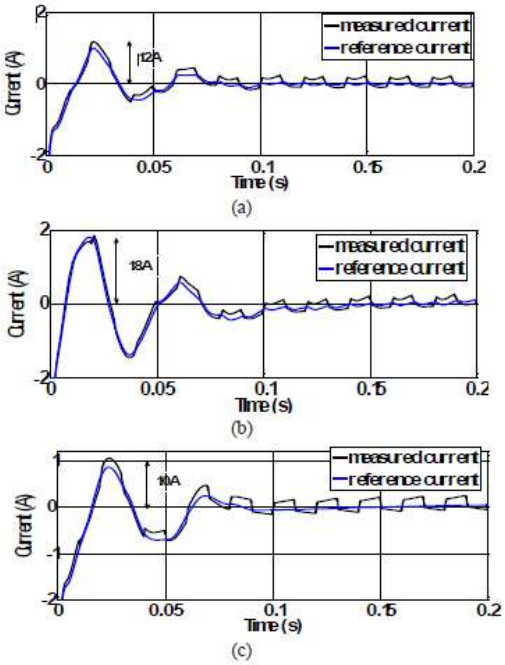

Fig. 6. Simulation waveform of the circulating current (a) based on the PI control method (b) based on the state-feedback method (c) based on the proposed state-feedback with the virtual impedance-loop method.

TABLE I

PARAMETERS OF THE MMC SYSTEM FOR SIMULATION AND EXPERIMENT

f	Fundamental frequency	50Hz
f_{sw}	Switching frequency	2kHz
R_f	AC coupling resistor	0.100Ω
L_f	AC coupling inductor	2mH
R_r	MMC buffer resistor	0.400Ω
L_r	MMC buffer inductor	2mH
C_d	Effective capacitor(s)	8000uF
V_{DC}	DC link voltage	130V
RL	Active -inductive Load (w/var)	50/50
V_{ref}	SM Reference voltage	30V
V_L	MMC output AC voltage	60V
$K1$	Proportional outer DC capacitor voltage gain	0.1
$K2$	Integral outer DC capacitor voltage gain	1.0
$K3$	Proportional capacitor voltage gain	0.5
$K4$	Proportional capacitor voltage gain	0.5
P	Proportional inner circulating current gain	0.3
I	Integral inner circulating current gain	3.0

The steady-state value of 0.5A of the circulating current based on the state-feedback method has been reached at approximately 0.10 sec. However, it can be seen from Fig. (b) that the state-feedback controller has a better reference tracking than that of the PI-control method.

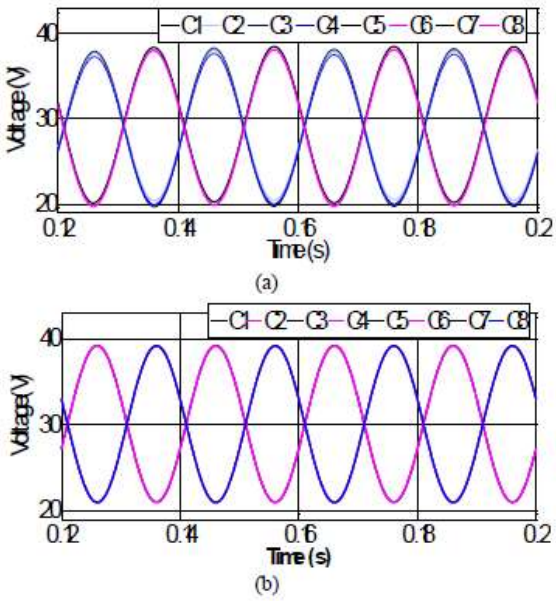

Fig. 7. Simulation waveforms of the SM capacitor voltages based on the (a) conventional method (b) proposed method

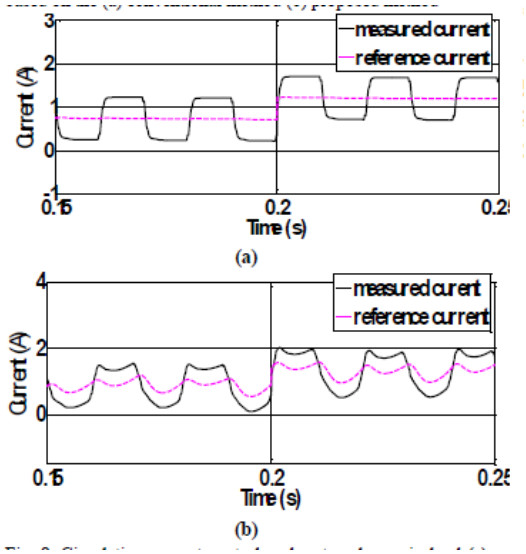

Fig. 8. Circulating current control under step-change in load (a) PI-control method (b) proposed method

From Fig. 6(c), it can be seen that the circulating current response of the virtual-impedance based the state-feedback control method has the smallest current overshoot of about 1.0A. In addition, both the reference and measured circulating current are less distorted. From Fig. 7 it can be seen that the capacitor voltages based on the PI-control method are more harmonic and have an estimated voltage ripple that is 2% higher than in the proposed method.

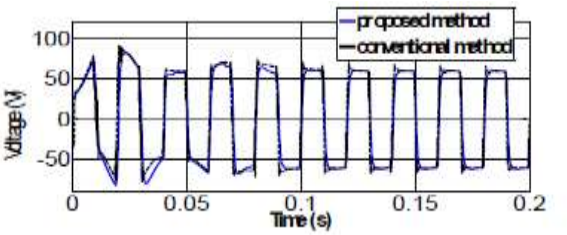

Fig. 9. Simulation waveforms of the single-phase output voltage based on conventional PI-control method and the proposed method.

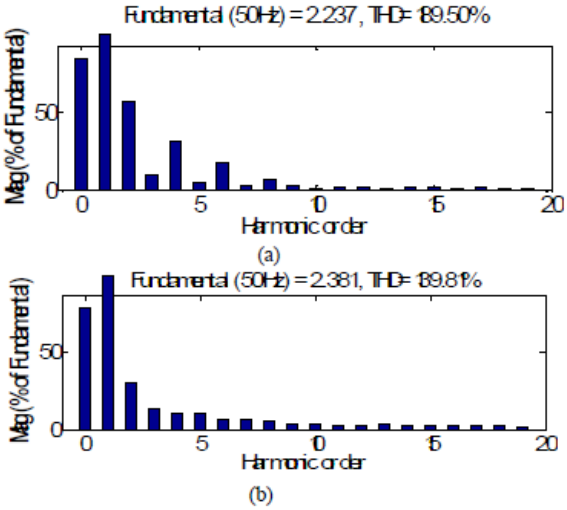

Fig. 10. Arm current spectrum (a) based on the PI control method (b) based on the proposed method.

The reduced capacitor voltage ripple has resulted in a less harmonic circulating and AC output voltage as shown in Fig. 8 and Fig. 9 respectively.

The responses in Figs 7, 8, 9 and 10 feature good tracking capability of the state-feedback controller when coupled with the voltage disturbance suppression using the virtual-impedance loop method. The less capacitor voltage variation feature of the proposed method can also be seen in the spectrum analysis of the arm current in Fig. 10. The dominate harmonics which are the even-order harmonics (second-order, forth-order and the sixth-order components) appeared to be reduced in magnitude compared to the values obtained based on the conventional method. It is seen from the spectrum analysis that the implementation of the proposed circulating current control method produced wideband opposing harmonic current components to the MMC operation from the feed-forward compensation.

5. EXPERIMENTAL RESULTS

A small setup is shown in Fig. 11. It is a single-phase proto-type of a five-level 250VA-MMC inverter with the system and control parameters that are given in Table I and Table II.

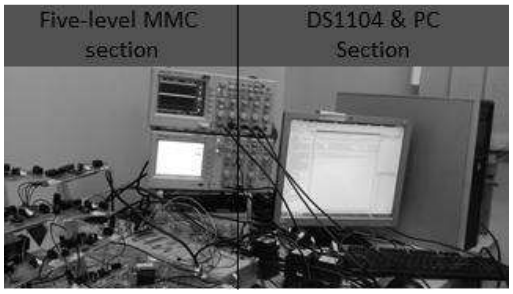

Fig. 11. Experimental set-up of the five-level MMC inverter system

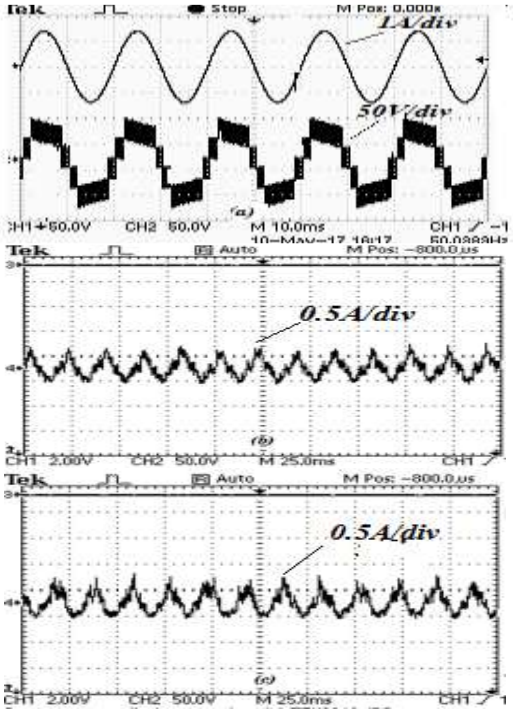

Fig. 12. Experimental waveforms (a) channel 1: load current channel 2: five-level output voltage using proposed method (b) circulating current based on the proposed method (c) circulating current based on the PI-control method.

The SM reference voltage is adjusted to 50V due to the number of the MMC level in the experiment. The control is implemented in the form of Simulink and executed using the ds1104 real-time controller.

Readings are captured using an oscilloscope and the CONTROL-Desk instrumentation. The MMC inverter output AC voltage and its output current, the SM capacitors voltages, circulating current, upper and the lower arm currents are measured and fed back through the dSPACE connector-panel to the personal computer (PC). Channel 1 of Fig. 12(a) shows how good waveform of the MMC output AC voltage with its output load current can be obtained based on the proposed method. Fig. 12(b) and (c) shows the circulating current obtained based on the proposed method and the PI-control method respectively. It is clear that the circulating current obtained based on the proposed method is less harmonic. However, the operation leads to emergence of low-magnitude low-order harmonics other than the second-order at slightly higher frequency range less than the switching frequency kHz. The simulation and the experimental results feature the efficiency of the proposed method in suppressing the effect of the voltage disturbance for an improved performance. However, this work could be improved by considering additional voltage disturbance term due to switching voltage ripple in (20) and incorporate it as part of the feedforward voltage. The inclusion of the voltage ripple will suppress the emergence of other harmonics especially around the switching frequency. This will be explored by the Authors in the future studies.

6. CONCLUSION

The voltage disturbance on the SM capacitor voltages leads to the generation of harmonics in the circulating current within the MMC system. This paper offers a concept of circulating current control of MMC with a state-feedback controller for a faster current response. The outer-loop average control in the proposed method is augmented with a virtual-impedance loop voltage. The performance of the state-feedback controller with the virtual impedance loop is compared with the performance of the conventional PI–controller. The obtained simulation results show the proposed method achieves an improved control with fewer harmonic without the increase in the SMCapacitors or buffer inductor sizes. The results from the two control schemes are presented. The experimental steady-state results have validated the proposed control.

REFERENCES

[1] P. Rao, M.L. Crow, Z. Yang, STATCOM control for power system voltage control applications, IEEE Trans. Power Deliv. 15 (2000) 1311–1317.

[2] K. Ilango, A. Bhargav, A. Trivikram, P.S. Kavya, G. Mounika, M.G. Nair, Power Quality Improvement using STATCOM with Renewable Energy Sources, Power Electron. (IICPE), 2012 IEEE 5th India Int. Conf. (2012) 1–6,.

[3] D.M. Reddy, Dynamic Performance of Power Quality Improvement Using Multilevel DSTATCOM with DG Application, (2014).

[4] A.U. Lawan, M. Student, H. Abbas, J.G.K.S. M, A.A. Karim, Dynamic performance of Improvement of MMC Inverter with STATCOM Capability interfacing PMSG Wind Turbines with Grid, 2015 IEEE Conf. Energy Convers. (2015) 492–497.

[5] A.U. Lawan, M. Mustapha, I. Abubakar, M. Mustapha, I. Abubakar, Reactive current control of STATCOM based MMC Inverter for Wind Turbines connected to Grid, 2015 IEEE Student Conf. Res. Dev. (2015) 26–31.

[6] L. Liu, H. Li, Y. Xue, W. Liu, Reactive power compensation and optimization strategy for grid-interactive cascaded photovoltaic systems, IEEE Trans. Power Electron. 30 (2015) 188–202. doi:10.1109/TPEL.2014.2333004.

[7] H. Wang, F. Blaabjerg, A. East, Reactive Power Compensation Capability of a STATCOM based on Two Types of Modular Multilevel Cascade Converters for Offshore Wind Application, (2017) 326–331.

[8] A.U. Lawan, N. Magaji, H. Musa, A STATCOM Controller for Small Signal Stability using Polynomial Algorithms in a Horizontal Axis Wind Farm Power System, 2013 IEEE Energytech USA. (2013) 1–5.

[9] N. Magaji, A.U. Lawan, A.D.O. Dan-isa, M.W. Mustafa, Design A STATCOM supplementary Controller for

Stability Studies using various state feedback algorithm,
Recent Res. Circuits Syst. (2012) 38–43.
[10] A.U. Lawan, State Feedback Approaches for Designing A Statcom Supplementary Controller for Oscillations Damping, Int. J. Eng. Sci. 3 (2014) 27–37.
[11] Y. Zhang, G.P. Adam, T.C. Lim, S.J. Finney, B.W. Williams, Analysis of modular multilevel converter capacitor voltage balancing based on phase voltage redundant states, IET Power Electron. 5 (2012) 726.
[12] M.M.C. Merlin, T.C. Green, Cell capacitor sizing in multilevel converters: cases of the modular multilevel converter and alternate arm converter, IET Power Electron. 8 (2015) 350–360.
[13] L. Norum, H. Nademi, Analytical circuit oriented modelling and performance assessment of modular multilevel converter, IET Power Electron. 8 (2015) 1625–1635.
[14] S. Liu, J. Jiang, Y. Wan, Generalised analytical methods and current-energy control design for modular multilevel cascade converter, IET Power Electron. 6 (2013) 495–504.
[15] R. Lizana, S. Member, M.A. Perez, S. Member, D. Arancibia, J.R. Espinoza, J. Rodriguez, Decoupled Current Model and Control of Modular Multilevel Converters, IEEE Trans. Ind. Electron. 62 (2015) 5382–5392.
[16] T. Poompavai, P.V. Priya, Comparative analysis of modified multilevel DC link inverter with conventional cascaded multilevel inverter fed induction motor drive, Energy Procedia. 117 (2017) 336–344.
[17] Z. Ahmad, S.N. Singh, An improved single phase transformerless inverter topology for grid connected PV system with reduce leakage current and reactive power capability, Sol. Energy. 157 (2017) 133–146.
[18] Z. Ahmad, S.N. Singh, Comparative analysis of single phase transformerless inverter topologies for grid connected PV system, Sol. Energy. 149 (2017) 245–271.
[19] Z. Ahmad, S.N. Singh, Single phase transformerless inverter topology with reduced leakage current for grid connected photovoltaic system, Electr. Power Syst. Res. 154 (2018) 193–203
[20] M. Miranbeigi, Y. Neyshabouri, H. Iman-Eini, State feedback control strategy and voltage balancing scheme for a transformer-less STATic synchronous COMpensator based on cascaded H-bridge converter, IET Power Electron. 8 (2015) 906–917.
[21] M. Zhang, L. Huang, W. Yao, Z. Lu, Circulating harmonic current elimination of a CPS-PWM-based modular multilevel converter with a plug-in repetitive controller, IEEE Trans. Power Electron. 29 (2014) 2083–2097.
[22] K. Shen, J. Wang, D. Zhao, M. Ban, Y. Ji, X. Cai, Investigation of capacitor voltage regulation in modular multilevel converters with staircase modulation, J. Power Electron. 14 (2014) 282–291.
[23] B. Li, D. Xu, D. Xu, Circulating current harmonics suppression for modular multilevel converters based on repetitive control, J. Power Electron. 14 (2014)
[24] H. Peng, Y. Wang, K. Wang, Y. Deng, X. He, R. Zhao, A Simple Capacitor Voltage Balancing Method with a Fundamental Sorting Frequency for Modular Multilevel Converters,14(2014) 1109–1118.
[25] R. Cisneros, M. Pirro, G. Bergna, R. Ortega, G. Ippoliti, M. Molinas, Global Tracking Passivity-based PI Control of Bilinear Systems and its Application to the Boost and Modular Multilevel Converters48 (2015) 420–425.
[26] Y. Chen, M. Wen, E. Lei, X. Yin, J. Lai, Z. Wang, Passivity-based control of cascaded multilevel converter based D-STATCOM integrated with distribution transformer, Electr. Power Syst. Res. 154 (2018) 1–12.
[27] G. Bergna, A. Garces, E. Berne, P. Egrot, A. Arzande, J.C. Vannier, M. Molinas, A generalized power control approach in ABC frame for modular multilevel converter HVDC links based on mathematical optimization, IEEE Trans. Power Deliv. 29 (2014) 386–394..
[28] G. Bergna, E. Berne, P. Egrot, P. Lefranc, A. Arzande, J.C. Vannier, M. Molinas, An energy-based controller for HVDC modular multilevel converter in decoupled double synchronous reference frame for

voltage oscillation reduction, IEEE Trans. Ind. Electron. 60(2013) 2360–2371.

[29] X. Wang, Y.W. Li, F. Blaabjerg, P.C. Loh, Virtual-Impedance-Based Control for Voltage-Source and Current-Source Converters, IEEE Trans. Power Electron. 30 (2015) 7019–7037.

[30] V.G. Agelidis, J. Pou, S. Ceballos, R. Darus, G. Konstantinou, Controllers for eliminating the ac components in the circulating current of modular multilevel converters, IET Power Electron. 9 (2016) 1–8.

[31] R. Li, J.E. Fletcher, A novel MMC control scheme to increase the DC voltage in HVDC transmission systems, Electr. Power Syst. Res. 143 (2017) 544–553.

[32] Y. Zhang, G.P. Adam, T.-C. Lim, S.J. Finney, B.W. Williams, Mathematical Analysis and Experiment Validation of Modular Multilevel Converters, J. Power Electron. 12 (2012) 33–39.

[33] N. Quach, S.H. Chae, S. Song, E. Kim, Frequency and Voltage Control Strategies of the Jeju Island Power System Based on MMC-HVDC Systems, 18 (2018) 204–211.

[34] A. Antonopoulos, L. Angquist, L. Harnefors, K. Ilves, H.-P. Nee, Global Asymptotic Stability of Modular Multilevel Converters, IEEE Trans. Ind. Electron. 61 (2014) 603–612.

[35] M. Hagiwara, H. Akagi, PWM control and experiment of modular multilevel converters, Power Electron. Spec. Conf. 2008. PESC 2008. IEEE. (2008) 154–161.

[36] K. Lee, T.M. Jahns, T.A. Lipo, V. Blasko, New Control Method Including State Observer of Voltage Unbalance for Grid Voltage-Source Converters, IEEE Trans. Ind.Electron. 57 (2010) 2054–2065.

[37] Q. Tu, Z. Xu, H. Huang, J. Zhang, T. Qingrui, X. Zheng, H. Hongyang, Z. Jing, Parameter design principle of the arm inductor in modular multilevel converter based HVDC, Power Syst. Technol. (POWERCON), 2010 Int. Conf. (2010) 1–6.

[38] S. Yang, S.M. Ieee, P. Wang, S.M. Ieee, Y. Tang, M. Ieee, Feedback Linearization Based Current Control Strategy for Modular Multilevel Converters, IEEE Trans. Power Electron. PP (2017) 161–174. doi:10.1109/TPEL.2017.2662062.

[39] L.H. HAF Mohamed, M Moghavvemi, Takagi-ugeno fuzzy gains scheduled PI controller for enhancement of power system stability, Am. J. Appl. Sci. 7 (1). pp. (2010) 145–152.

[40] S.Y. LH Hassan, HAF Mohamed, M Moghavvemi, Automatic generation control of power system with fuzzy gain scheduling integral and derivative controller, Int. J. Power, Energy Artif. Intell. 1,1 (2008) 29–33.

[41] L.K. Haw, M.S.A. Dahidah, S. Member, H.A.F. Almurib, S. Member, A New Reactive Current Reference Algorithmfor the STATCOM System Based on Cascaded Multilevel Inverters, IEEE Trans. POWER

[42] A. U. Lawan, Babani, A. Abdulkarim, G. S. Shehu, Y. Jibril, I. S. Madugu, ―Power Compensation for Vector-based Current Control of a Modular Multilevel Converter (MMC) based STATCOM‖ International Journal of Power Electronics and Drives (IJPEDS) vol.10, no. 4, pp. 71~85, 2019).

[43] A. U. Lawan, Haider A.F. Almurib, Jeen G. Khor ―Modular Multilevel Converter (MMC) based STATCOM with Vector Control and Virtual Impedance Voltage Compensations‖ International Journal of Power Electronics and Drives (IJPEDS), vol. 10, no. 4, pp. 51~70, 2019.

[44] A. U. Lawan, H. Abbas, J. G Khor , ― Enhanced decoupled Current Control with Voltage Compensation for Modular Multilevel Converter (MMC) based STATCOM‖ International journal of Power Electronics and Drives (IJPEDS) vol.10, no.3, pp.1483-1499, 2019.